Original Article

Open Guided Waves: online platform for ultrasonic guided wave measurements

Jochen Moll[1] [iD], Jens Kathol[2], Claus-Peter Fritzen[2], Maria Moix-Bonet[3], Marcel Rennoch[4] [iD], Michael Koerdt[4], Axel S Herrmann[4], Markus GR Sause[5] and Martin Bach[6]

Abstract

Ultrasonic guided waves have been used successfully in structural health monitoring systems to detect damage in isotropic and composite materials with simple and complex geometry. A limitation of current research is given by a lack of freely available benchmark measurements to comparatively evaluate existing methods. This article introduces the extendable online platform Open Guided Waves (http://www.open-guided-waves.de) where high-quality and well-documented datasets for guided wave-based inspections are provided. In this article, we describe quasi-isotropic carbon-fiber-reinforced polymer plates with embedded piezoelectric transducers as a first benchmark structure. Intentionally, this is a structure of medium complexity to enable many researchers to apply their methods. In a first step, ultrasound and X-ray measurements were acquired to verify pristine conditions. Next, mechanical testing was done to determine the stiffness tensor and sample density based on standard test procedures. Guided wave measurements were divided into two parts: first, acoustic wave fields were acquired for a broad range of frequencies by three-dimensional scanning laser Doppler vibrometry. Second, structural health monitoring measurements in the carbon-fiber-reinforced polymer plate were collected at constant temperature using a distributed transducer network and a surface-mounted reversible defect model. Initial results serving as validation are presented and discussed.

Keywords

Guided waves, composite structures, signal processing, structural health monitoring, scanning laser Doppler vibrometry

Introduction

A literature review published by Mitra and Gopalakrishnan[1] shows the recent developments in the area of guided wave techniques for structural health monitoring (SHM). Multiple methods were reported in that paper ranging from signal processing techniques to statistical and machine learning methods. The important question for the practical application of guided wave–based diagnostics is the performance of the methods relative to each other. In other words, what is the diagnostic accuracy of those methods, for example, in terms of damage detection sensitivity and localization correctness.

The lack of permanent and publicly available benchmark models motivated the research presented in this article. By means of well-documented and freely accessible measurements, existing algorithms for SHM and wave field processing can be fairly compared without

[1]Department of Physics, Goethe University Frankfurt, Frankfurt am Main, Germany
[2]Department of Mechanical Engineering, University of Siegen, Siegen, Germany
[3]Institute of Composite Structures and Adaptative Systems, Multifunctional Materials, German Aerospace Center (DLR), Germany
[4]Measurement Systems and Monitoring, Faserinstitut Bremen e.V. (FIBRE), Bremen, Germany
[5]Mechanical Engineering, Institute for Materials Resource Management, University of Augsburg, Augsburg, Germany
[6]ETLN—NDT Engineering & Process Simulation, Airbus Helicopters Deutschland GmbH, Donauwörth, Germany

Corresponding author:
Jochen Moll, Department of Physics, Goethe University Frankfurt, Max-von-Laue-Straße 1, 60438 Frankfurt am Main, Germany.
Email: moll@physik.uni-frankfurt.de

uncertainties related to different measurement equipment, different transducer technology, and so on. In this sense, such datasets might be considered as a reference standard. The data base might also be helpful for guided wave beginners and those researchers with smart ideas but no access to expensive measurement equipment. The overall goal of the Open Guided Waves (OGW) online platform is to support research and developments in the field of guided wave technology for SHM.

Basically, SHM methods must be at least as reliable as competing non-destructive testing (NDT) techniques.[2,3] To proof reliability, appropriate requirements for damage detection need to be defined and validated with respect to the structural items of interest. This process is well established for the verification or "technical qualification" of conventional ultrasonic testing.[4,5] For active guided wave approaches, the differences are in the required elaborate consideration of structural features at the structural item, variations of environmental and operational conditions (EOCs) in conjunction with a potential dependency on previous measurement data (e.g. reference or baseline data), and the interaction of guided waves with structural damage in terms of damage type, position, and inspection frequency.[6–8]

Most current works only partly address those aspects. There are major differences in numerical modeling procedures or the way experiments were performed. Due to this high degree of variation, a comparison of results is nearly impossible, for example, due to different modeling strategies, or different actuators and data acquisition systems used. This shows the need to establish benchmark tests that are valuable to compare and validate guided wave–based methods for SHM.

The underlying idea of the proposed OGW platform is shown in Figure 1 which illustrates the whole process from data acquisition to its distribution. A first test structure, described in section "Description and characterization of the test structures," is given by carbon-fiber-reinforced polymer (CFRP) plates with clearly defined geometry and embedded piezoelectric transducers. To characterize the baseline state, ultrasound and X-ray testing were performed. Material properties in the form of stiffness tensor and sample density were measured, validated, and compared with theoretical predictions. A discussion of the reversible damage model used in this work is presented in section "Relevance of reference damage." Next, section "Guided wave measurements part I: 3D acoustic wave field measurements" describes the acoustic wave field measurements by a three-dimensional (3D) scanning laser Doppler vibrometer characterizing guided wave propagation in the structure for a broad range of frequencies. This dataset will be helpful in the verification of numerical methods simulating wave propagation in
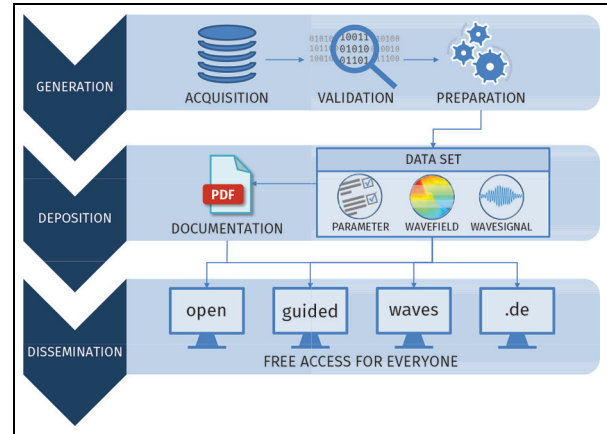

Figure 1. Workflow illustrating data generation, deposition, and dissemination.

composite materials.[9–16] This wave field data are also beneficial for the verification of image processing tools for acoustic wave field analysis and spectroscopy.[17–22] Section "Guided wave measurements part II: SHM measurements" presents the SHM measurements of the CFRP plate at constant temperature where a surface-mounted reversible defect model was placed at several positions on the structure. Multiple frequencies were recorded in a round-robin fashion at each structural condition. This dataset is well suited to test baseline-dependent and baseline-free damage detection and damage localization methodologies.[23–27] Finally, conclusions are drawn at the end in section "Summary."

Description and characterization of the test structures

Test structure preparation

Four CFRP plates were manufactured for this study with the dimensions of 500 mm $\times$ 500 mm and a thickness of 2 mm. The specimens are based on prepreg material Hexply® M21/34%/UD134/T700/300. Depending on its purpose, as shown in Table 1, the laminates are either quasi-isotropic with layup $[45/0/-45/90/-45/0/45/90]_S$ or unidirectional.

A first specimen, called "wave field plate," with a single piezoelectric transducer in the center was used for acoustic wave field measurements. A second specimen, called "SHM plate," was equipped with 12 piezoelectric transducers for the acquisition of guided wave data in pitch-catch configuration. Both specimens are shown in Figure 2. Two additional laminates are divided in coupons and undergo mechanical testing to determine the material properties, and to validate the stiffness tensor.

DuraAct piezoelectric transducers are co-bonded to the plate during the curing process in the autoclave. These transducers are composed of a lead zirconate

Table 1. Labeling and description of the laminates.

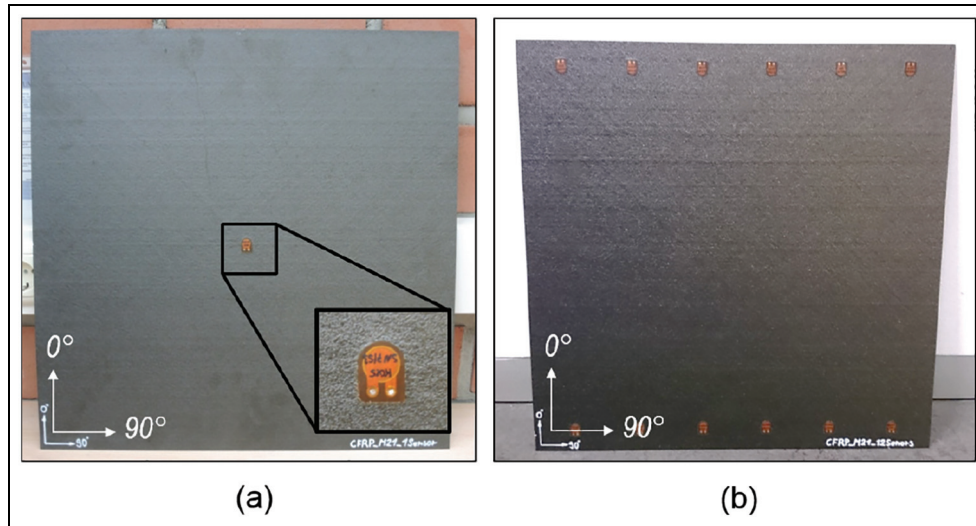| No.	Layup	Transducers	Labeling	Purpose
1	Quasi-isotropic	12	"SHM plate"	Acousto-ultrasonics
2	Quasi-isotropic	1	"Wave field plate"	Full-wave field analysis
3	Unidirectional	No	–	Mechanical testing (stiffness tensor measurement)
4	Quasi-isotropic	No	–	Mechanical testing (validation)

Figure 2. (a) "Wave field plate" with single transducer in the middle of the structure; (b) "SHM plate" equipped with 12 transducers. One row with six equally spaced transducers is arranged on top and one row at the bottom of the plate. In both plates, the horizontal direction denotes a fiber orientation of 90° and the vertical direction represents a fiber orientation of 0°.

titanate (PZT) circular disk embedded in a ductile polymer along with the required electrodes, electrical contacts, and insulators.[28] The piezoelectric disk measures 0.2 mm in thickness and 5 mm in diameter. The embedding of the piezoelectric transducer provides electrical insulation and mechanical pre-compression, making the piezoceramic robust against deformations. The capacitances of the 12 transducers of the "SHM plate" are listed in Table 2 and show only small variability.

Baseline state characterization using ultrasonic testing. All specimens were inspected by ultrasonic NDT to verify the undamaged state. The inspection has been performed with a USPC 3040 ultrasonic imaging system (Ingenieurbüro Dr. Hillger, Braunschweig, Germany) equipped with a 5-MHz transducer (Olympus V309) by means of immersion testing in pulse-echo configuration.

Figure 3 depicts the amplitude of the backwall echo in decibels for the "SHM plate." The specimen has been evaluated for damage following the 6-dB method described in Schnars and Henrich[29] and Brandt and

Table 2. Capacitance of piezoelectric disks of the "SHM plate" measured with PeakTech Capacitance Tester 3710.

Transducer	Capacitance (nF)
T_1	4.54
T_2	4.52
T_3	4.58
T_4	4.54
T_5	4.45
T_6	4.60
T_7	4.51
T_8	4.41
T_9	4.56
T_{10}	4.53
T_{11}	4.59
T_{12}	4.60

Maaß.[30] In that technique, a composite laminate is considered damage-free if the backwall echo does not drop 6 dB or more in comparison with a defect-free area within the same material, thickness, and stacking sequence. The amplitude of the backwall echo in Figure 3 remains between -4 and -10 dB, indicating the pristine state of the specimen.
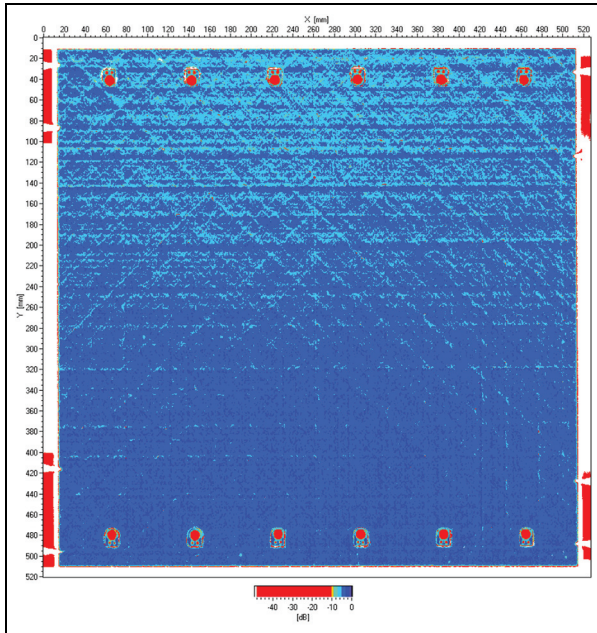
Figure 3. Backwall echo of ultrasonic NDT of the "SHM plate" with 12 co-bonded piezoelectric transducers.

Baseline state characterization using X-ray testing. Industrial radiography and computed tomography (CT) are well established in material science for non-destructive evaluation of technical components to detect defects such as cracks, delaminations, or voids.[31] The object of interest is placed between an X-ray tube and an array detector. As different materials variously absorb the X-rays passing through it, a grayscale image can be generated,

representing attenuation of X-rays in each pixel. This is why regions of higher density appear brighter and are distinguishable from material parts with lower X-ray density.

Digital radiography was performed in this work for the "wave field plate" and the "SHM plate" using a phoenix v|tome|x m (research edition) CT, developed by GE Sensing & Inspection Technologies GmbH (Wunstorf, Germany). This instrument is equipped with both a microfocus X-ray tube with a reflection target up to a maximum of 240 kV at 320 W and a nanofocus X-ray tube with a transmission target up to a maximum of 180 kV at 15 W. The test structures were exposed for 500 ms to a beam, emitted from the microfocus tube with a source voltage of 50 kV and a source current of 130 μA. According to the US standard ASTM E2597-07, the X-rays passing through are then detected by a temperature-stabilized digital GE DXR detector array, with 2000 × 2000 pixels of size 200 μm on a 400 mm × 400 mm surface. The signal-to-noise ratio was further increased by averaging five frames per image after one skip.

Figure 4 shows the X-ray images for the "wave field plate" and the "SHM plate." Both images show a black region at the bottom corresponding to the sample holder to fix the sample during radiographic measurements. A soft masking tape protects the bottom edge of the plate, which can be seen as a dark shade around the holding device. The piezoelectric transducers can be clearly identified by their black shape. To provide orientation for the "SHM plate," an upward arrow of copper tape was bonded onto the surface and, hence,
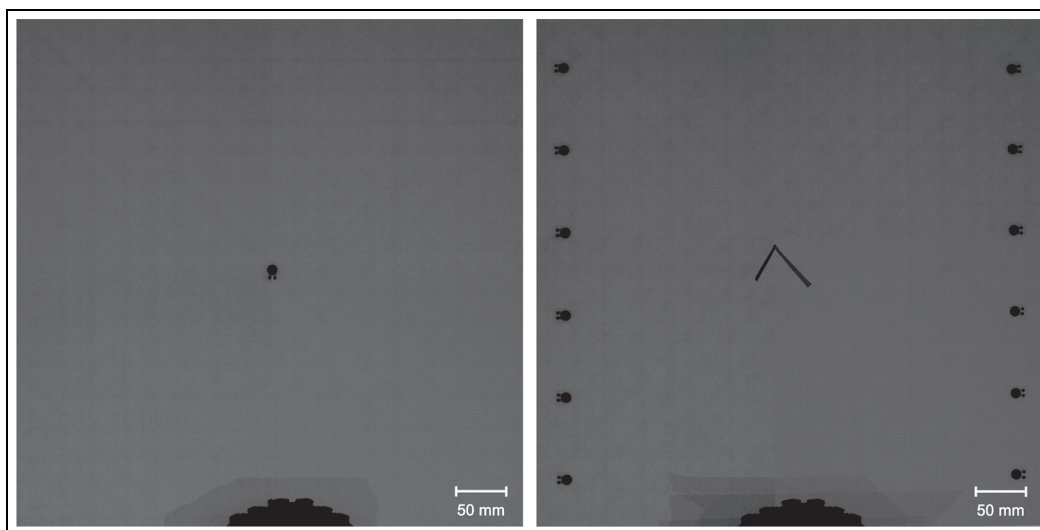

Figure 4. X-ray images of the "wave field plate" (left) and the "SHM plate" (right). The black region at the bottom of both images corresponds to the sample holder used to fix the samples during X-ray measurements. The "SHM plate" shows an upward arrow of copper tape in the center of the plate that was bonded to the specimen to provide correct orientation.

Table 3. Measurement values and test standards used to obtain material properties.

Quantity	Value	Test standard	Source
E_{11}	125.5 ± 2.4 GPa	DIN EN ISO 527-5	–
E_{22}	8.7 ± 0.1 GPa	DIN EN ISO 527-5	–
G_{12}	4.135 GPa	EN ISO 14129	Petersen et al.[32]
ν_{12}	0.37 ± 0.08	DIN EN ISO 527-5	–
ν_{23}	0.45 ± 0.02	DIN EN ISO 527-5	–
ρ	1571 ± 2 kg/m^3	–	–

can be recognized in the center of the corresponding image. In addition, in both images, lines in the direction angles 0°, 90°, and ±45° occur, indicating the directions of the laminate plies. Note that there are no further grayscales, which differ from the homogeneous gray that is generated by the unvarying absorption of the material. Commonly, this is considered as intact in the range of the given resolution. Therefore, it is noteworthy that in fact there may be defects smaller than the provided resolution of 120 μm. However, those will have no influence on the wave propagation due to the chosen ultrasound wavelength. Hence, both samples are assumed as intact, that is, suitable to provide baselines for further characterization.

Mechanical parameter measurement

In order to implement modeling of guided waves for fiber-reinforced laminates, the stiffness tensor and the density of the material are required. In this study, we establish the stiffness tensor for the unidirectional plies of the Hexply M21/34%/UD134/T700/300 material used for fabrication of the test structure. This is partly based on measurements and partly based on literature values published for this batch of this material.[32]

Table 3 lists the measured material properties as well as the corresponding test standards. All material samples were conditioned and tested at 23°C and 50% relative humidity (RH), to obtain material properties at the same test conditions as used for measurements of the "wave field plate" (see section "Guided wave measurements part I: 3D acoustic wave field measurements") and "SHM plate" (see section "Guided wave measurements part II: SHM measurements"). All tests were conducted in accordance with the corresponding standards, except for the use of digital image correlation techniques for strain measurements. To obtain the ν_{23} Poisson's ratio, the strain field was evaluated at the edge of the laminate (cf. approach presented in Sause[33]).

Applying the Maxwell–Betti relationship[34] for E_{11}, E_{22}, ν_{12}, and ν_{21}

Table 4. Values of stiffness tensor for unidirectional Hexply M21/34%/UD134/T700/300 material.

Unidirectional laminate (GPa)
$C_{11} = 130.0$
$C_{12} = C_{13} = 6.1$
$C_{23} = 5.2$
$C_{22} = C_{33} = 11.2$
$C_{44} = 3.0$
$C_{55} = C_{66} = 4.2$

$$\frac{E_{11}}{\nu_{21}} = \frac{E_{22}}{\nu_{12}} \tag{1}$$

and the in-plane relationship of E_{22}, E_{23}, and G_{23} is

$$G_{23} = \frac{E_{22}}{2(1 + \nu_{23})} \tag{2}$$

which leads to the stiffness tensor of the unidirectional layer as listed in Table 4.

Validity of the stiffness tensor was evaluated by tensile tests following DIN EN ISO 527-4 using off-axis angle measurements at incremental angles of 15° for a quasi-isotropic plate. Within the margin of error, the calculated values coincide with the measurement results (cf. Figure 5(a)). For the test frequency of 50 kHz, the phase velocity was extracted from full-field laser vibrometer measurements (see section "Guided wave measurements part I: 3D acoustic wave field measurements"). The result is compared to phase velocities calculated by finite element modeling following the approach in Sause[35] and shown in Figure 5(b). Within the margin of error, these calculations agree reasonably well with the experimental results. The obtained stiffness tensor may thus be assumed valid for the test conditions of the "wave field plate" in section "Guided wave measurements part I: 3D acoustic wave field measurements" and the "SHM plate" in section "Guided wave measurements part II: SHM measurements."
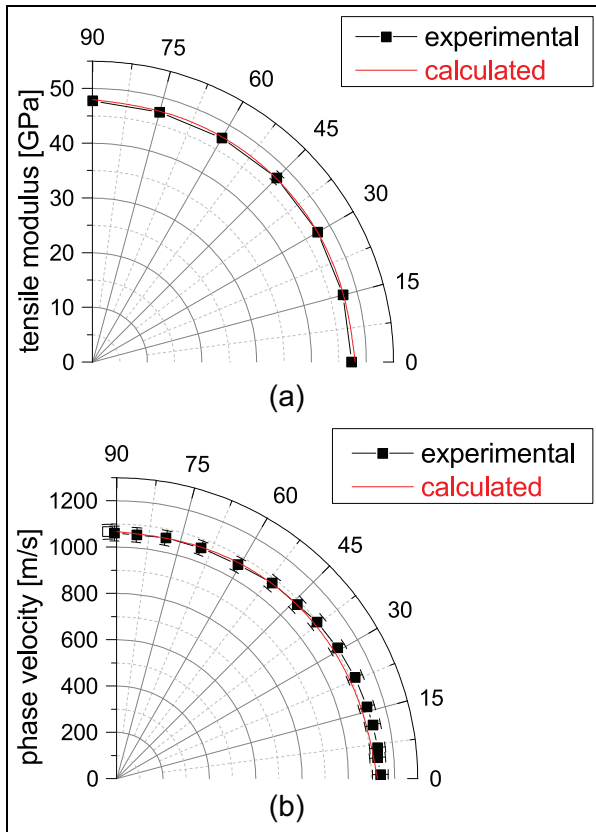
Figure 5. (a) Comparison of stiffness values predicted by classical laminate theory and measurement values at 15° angle increment for static tests and (b) comparison of phase velocity obtained by finite element modeling at 50 kHz and obtained by full-field laser vibrometer measurements.

In addition, the theoretical group velocities were computed by the well-known global matrix method exploiting third-order plate theory.[36] The third-order plate theory agrees well with the exact 3D theory, especially at lower frequency-thickness products.[37] A polar representation of the group velocity for three representative frequencies is shown in Figure 6. Given by the quasi-isotropic stacking sequence, the velocity is almost independent of the direction of wave propagation.

Relevance of reference damage

The propagation of guided ultrasonic waves in CFRP material is adequately described, for example, in Rose,[38] Su et al.,[39] and Wang and Yuan.[40] For simplified cases, the interaction of guided waves with damage can be modeled as well, as shown for a symmetric delamination in Ramadas et al.[41] The geometry of a realistic impact damage is more complex, usually described with a pine-tree-shaped delamination with additional matrix and fiber cracks.[42] The interaction of guided waves with realistic damages is of high importance for verification of damage detection and assessment reliability, as the underlying algorithm needs to extract appropriate features from this interaction.

Giving an example for conventional ultrasonic inspection, appropriate features are the occurrence of intermediate echoes between interface echo and backwall echo, or the attenuation of the backwall echo. Both features are very stable and easy to analyze. This means that reference measurements can be done on any structure with similar thickness, attenuation, and wave velocity. In addition, ultrasound features can be easily reproduced by flat bottom holes or a separating foil.[43]

By transferring this example to guided wave propagation, the conceptual differences become clearer: As most state-of-the-art algorithms for damage detection or assessment are using a baseline subtraction method,
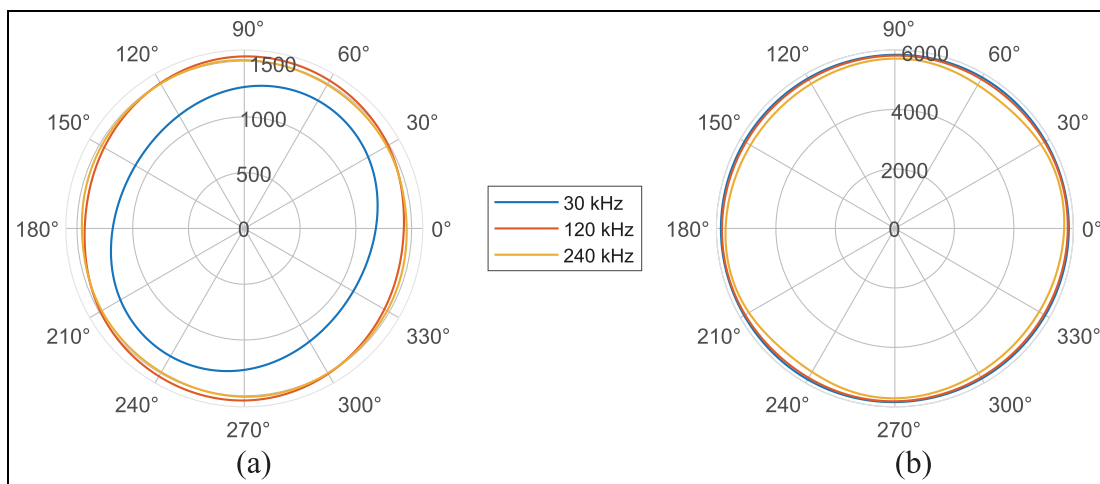

Figure 6. Polar representation of the group velocity (m/s) for (a) the A_0-mode and (b) the S_0-mode. The frequencies shown here reflect the minimum, intermediate, and maximum frequencies during the experiments of the undamaged "wave field plate" (see Table 5).
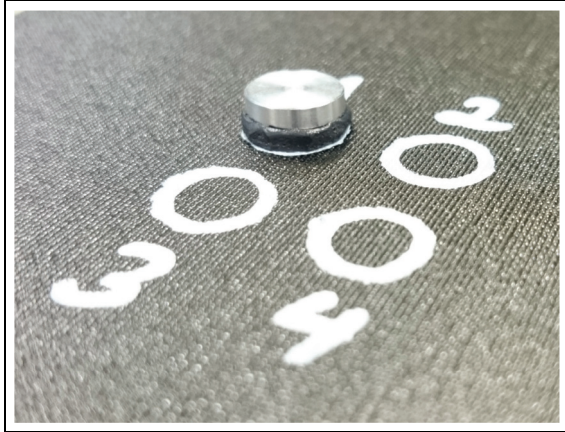
Figure 7. Photograph of the reversible damage model in the form of an aluminum disk with a diameter of 10 mm coupled to the structure by tacky tape. White circles indicate four closely spaced damage positions (cf. Figure 12).

Figure 8. Experimental setup with the scanning laser Doppler vibrometer and the "wave field plate."

the reference measurement needs to be done on a very silmilar structure or even the structure itself with same EOC. Even more important are the features for damage identification that can be different as soon as the damage type changes.

In this work, we employ a reversible defect model where an aluminum disk is mounted on the surface of the CFRP plate by a tacky tape as introduced in Beard et al.[44] (cf. Figure 7). Although this reference damage is simplified with respect to the geometry of an actual delamination, its interaction with guided waves behaves similarly in terms of dedicated features such as change in time of flight or decrease in amplitude as quantified in Bach et al.[45]

The underlying idea of using this reversible damage is to provide measurement data at various places on the structure so that model-assisted probability of detection (MAPOD) techniques can be developed.[7,8]

Table 5. Carrier frequencies used for acoustic wave field measurements.

Description	Carrier frequencies (kHz)
Undamaged structure	30–100 ($\Delta f = 10$)
	120–240 ($\Delta f = 20$)
Damaged structure	30, 50, 100, 150, 200, and 250

The reference damage (see Figure 7) was placed at location $x = -0.059$ m and $y = 0.045$ m (in the coordinate system of the laser Doppler vibrometer setup shown in Figure 10).

Guided wave measurements part I: 3D acoustic wave field measurements

As shown in Figure 8, full-wave field measurements were carried out by a 3D scanning laser Doppler vibrometer PSV-400-3D from Polytec GmbH (Waldbronn, Germany) using a measurement range of ± 200 mm/s. To increase sampling rate to 2.56 MHz, the PCI 6110 National Instruments measurement card was used. Measurement subject was the "wave field plate" introduced before with a central transducer placed exactly in the middle of that structure. The excitation signal is a 5-cycle Hann-filtered sine wave amplified to ± 150 V. To minimize the influence of random

measurement noise, every dataset is averaged 100 times. The temperature was kept constant at room temperature, in this case, 23°C.

Many experiments have been performed on the "wave field plate" for the undamaged and the damaged specimen as listed in Table 5. The carrier frequencies in the experiments range from 30 to 240 kHz in steps of Δf. The reference damage shown in Figure 7 is used to model a structure with a defect. For reasons of symmetry, only the lower-left quarter of the plate was examined. Hence, the transducer is located in the upper-right corner of the measured wave field.

Figure 9 depicts the measured wavenumbers of the "wave field plate" along 0° direction (see Figure 2) as a
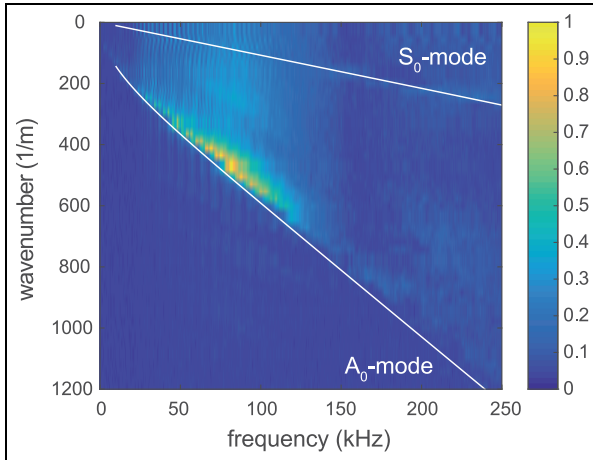
Figure 9. Comparison between theoretically predicted and experimentally measured dispersion properties of the "wave field plate" in 0° direction (see Figure 2). Multiple narrowband measurements were combined to model a broadband pulse. The experimental dispersion graph was normalized to the maximum amplitude of the antisymmetric wave mode. Theoretical dispersion curves were computed with the global matrix method.[36]

Figure 10. Snapshot of the acoustic wave field excited at 50 kHz after 155.8 µs. Snapshot (left) for the undamaged structure and (right) the damaged structure showing antisymmetric wave mode scattering at the defect. The damage position is marked by a red circle.

result of a 2D Fourier transform in relation to theoretically predicted dispersion curves in the multilayered laminate. The theoretical dispersion curves are in good agreement with the experimental dispersion curves. In addition, mode tuning behavior can be observed which describes the capability of piezoelectric transducers to excite and detect Lamb waves.[46] In the present case, the maximum of A_0-mode excitation is in the region of about 80 kHz and decreases to lower and higher frequencies, respectively.

In addition, Figure 10 shows the snapshots measured at 50 kHz for the intact structure and for the structure with the reference damage placed at $x = -0.059$ m and $y = 0.045$ m. Antisymmetric wave mode scattering can be clearly observed.

Guided wave measurements part II: SHM measurements

Figure 11 shows the experimental setup with the "SHM plate" placed in a climate chamber at a constant temperature of 23°C and 50% RH (DIN EN ISO 291). On the top and at the bottom of the structure, Pt-100 temperature sensors were attached to the plates' surface to assess potential temperature gradients. The temperature sensors were coupled to a PT-104A device (Omega Engineering GmbH, Deckenpfronn, Germany) that allows temperature measurements with a resolution of 0.001°C and an accuracy of 0.01°C. One temperature measurement was recorded for each dataset. Similar to
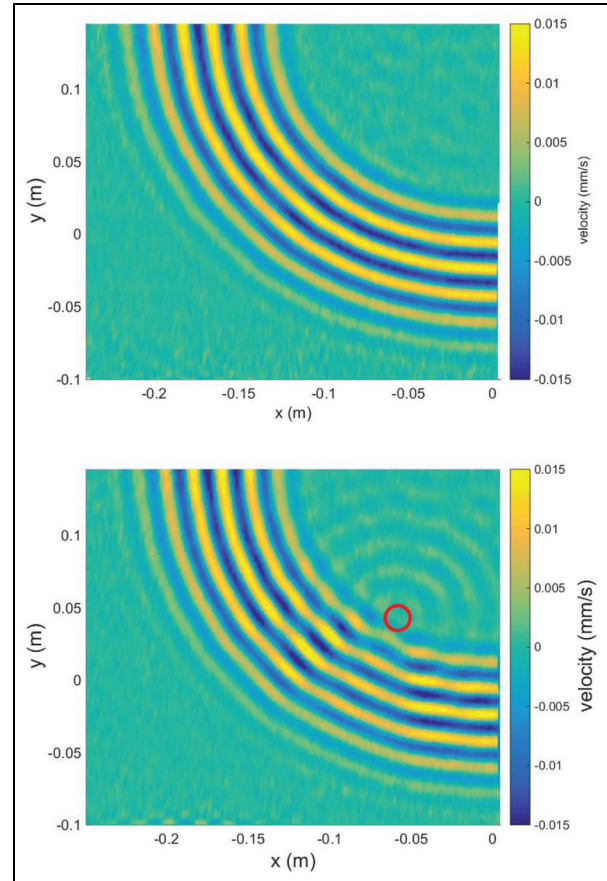
the wave field measurements described in the previous section, a Hann-filtered sine wave with 5 cycles was used with an amplitude of ±100 V. A dedicated device described in Neuschwander et al.[47,48] acquires all actuator–sensor pairs in a round-robin fashion, that is, time-division multiplexing.

The process of data acquisition for the SHM measurements is listed in Table 6 and consists of six phases. In the first phase, 20 baseline measurements of the intact structure were recorded. After that, the model defect was placed at 11 different positions on the plate. These measurements correspond to damage positions D_1 to D_{11} as shown in Figure 12. In each case, only a single defect model is attached to the structure at the same time. Another 20 baseline measurements were recorded in the third phase, followed by measurements of damage positions D_{12} to D_{20} in phase 4. Phase 5 consists of 20 additional baseline measurements of the pristine structure. The large number of baseline measurements enables the analysis of statistical variations
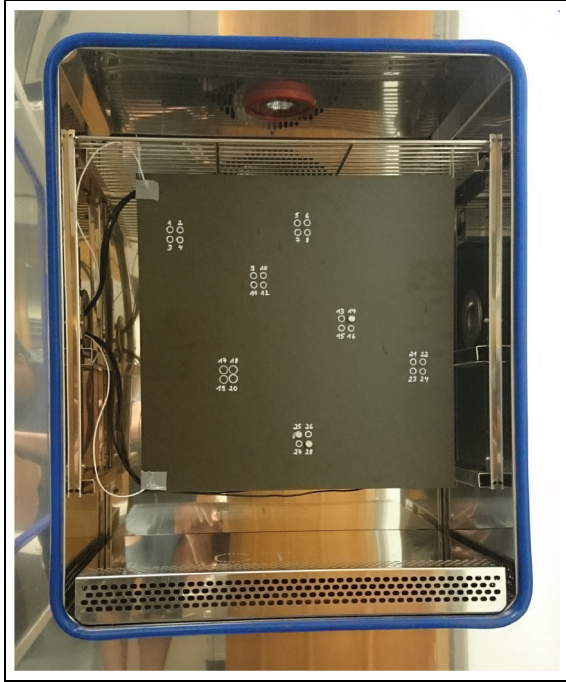
Figure 11. Photograph of the "SHM plate" in the climate chamber, where the tests were performed at 23°C and 50% RH. Two temperature sensors were installed on the top left and bottom left to measure the surface temperature of the samples.

Table 6. Process of data acquisition for the SHM measurements.

Phase	Description
1	20 baseline measurements
2	Damage scenarios D_1 to D_{11}
3	20 baseline measurements
4	Damage scenarios D_{12} to D_{20}
5	20 baseline measurements
6	Damage scenarios D_{21} to D_{28}, D_{25}/D_{28}, and $D_{14}/D_{25}/D_{28}$

in the baseline measurements, compared with Attarian et al.[49] who studied the baseline changes in the case of temperature variations. In the last phase, damage positions D_{21} to D_{28} were measured, plus two additional datasets with two and three concurrent surface defects.

The data acquisition took about 3 days. During that time, the temperature in the climate chamber was quite stable with a maximum temperature variation of 0.49°C (sensor on top) and 0.37°C (sensor at the bottom). This means that temperature compensation techniques, such as the ones proposed by Croxford et al.[50] or Douglass and Harley,[51] are not needed here.
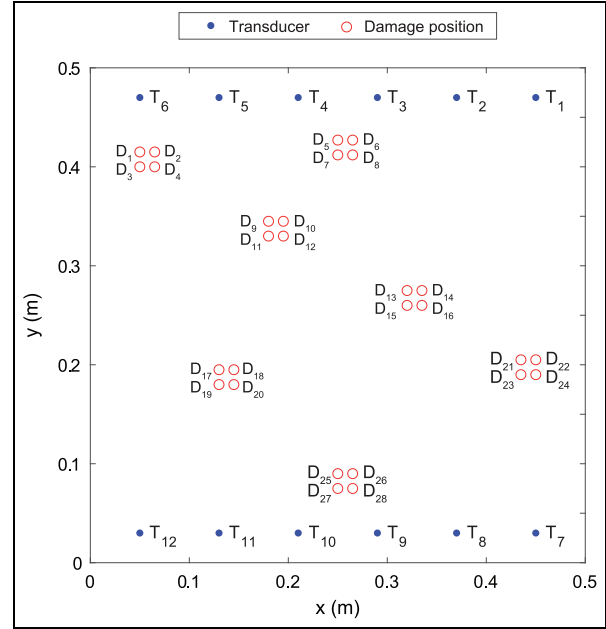

Figure 12. Geometry of the transducer positions T_1 to T_{12} and the defect locations D_1 to D_{28} during the SHM measurements.

Figure 13 depicts the exemplary guided wave measurements at 60 kHz for the transducer pairs $T_1 - T_7$ and $T_6 - T_{12}$. Please note that the geometry of the transducer pairs is symmetric for this case with respect to the boundary of the plate (cf. Figure 12). This leads to similar time-domain signals from both transducer pairs. The signals marked in blue correspond to 60 unique baseline measurements from the undamaged structure including datasets from phases 1, 3, and 5. The signal marked in red corresponds to a measurement where the model defect was placed at damage position D_1 (in the path of transducer pairs $T_6 - T_{12}$). It is interesting to see from the differential representation shown at the bottom of Figure 13 that the measured signals for the intact structure is almost pure measurement noise while a distinct waveform can be observed in the differential signal of the damaged structure. This waveform corresponds to guided wave scattering at the defect, mainly based on the interaction of the fundamental antisymmetric wave mode with the surface damage. This leads to changes in the measured signals with respect to the baseline signals that can be analyzed for damage assessment.

The reconstruction algorithm for probabilistic inspection of damage (RAPID), described by Hay et al.,[52] is well known as a damage localization technique in composite materials. This method was used here to demonstrate the localization capability of guided waves in the proposed CFRP plate. Figure 14 shows the two exemplary image reconstruction results based on
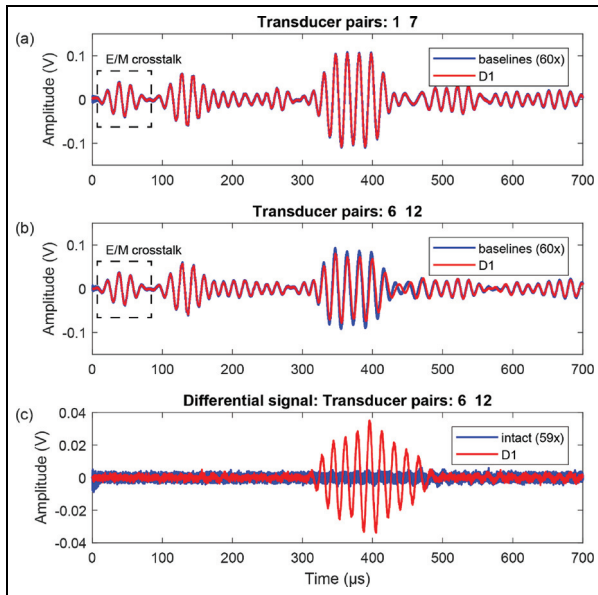
Figure 13. (a, b) Sixty Guided wave measurements at 60 kHz from the intact structure (marked in blue) and one guided wave measurement from the damaged structure (marked in red) for two different transducer pairs. (c) Differential signal after baseline subtraction. While the differential signals from the intact structure are measurement noise only, a distinct waveform can be observed in the differential signal due to wave scattering at the defect corresponding to damage case D_1. All signals were high-pass filtered using a Butterworth filter with a filter order of $n_F = 3$ and a cut-off frequency of 20 kHz.

40 kHz measurements. It is shown that damage D_4 and D_{16} were localized in both cases. In the analysis, only those datasets that have transducer pairs on opposite sides (top and bottom) were included, that is, where the damage is in the direct path of an actuator and its corresponding sensor.

Summary

This article introduced the OGW platform with a first benchmark dataset from quasi-isotropic CFRP plates with embedded piezoelectric transducers. The article described the fabrication of the test structures as well as their characterization by means of ultrasound and X-ray testing. In addition, the stiffness tensor and the density of the samples were measured and documented, and verified by numerical simulations and experimental measurements.

Acoustic wave field measurements for multiple frequencies were performed on the so-called "wave field plate," where a single piezoelectric transducer was placed in the middle of the test structure. Initial analysis showed good agreement between experimentally and theoretically predicted dispersion properties. Subsequent measurements on the "SHM plate" were conducted at constant temperature conditions in a climate chamber. The analysis showed the high quality of differential signals as well as the possibility for damage localization employing guided wave tomography techniques.

All guided wave measurements can be downloaded freely from the project's website (http://www.open-guided-waves.de) in HDF5 format supported by example scripts. Based on these datasets, existing guided wave techniques can be comparatively evaluated. Future work aims at additional datasets for the OGW platform including measurements with a more complex geometry or recorded under changing EOCs. The OGW platform is open for contributions from researchers worldwide. Most important are the technical quality, scientific rigor, same file format, and soundness of a preliminary analysis.
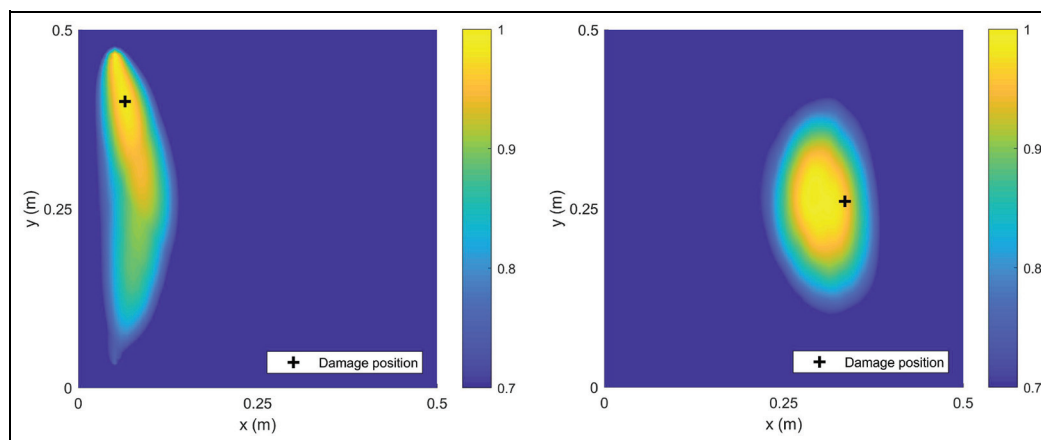

Figure 14. Guided wave tomographic image reconstruction at 40 kHz for damage D_4 (left) and damage D_{16} (right). The scaling parameter of the RAPID algorithm was defined here as $\beta = 1.1$.

Acknowledgements

Declaration of conflicting interests

Funding

ORCID iDs

Jochen Moll https://orcid.org/0000-0003-2299-2250
Marcel Rennoch https://orcid.org/0000-0001-7183-561X

References

1. Mitra M and Gopalakrishnan S. Guided wave based structural health monitoring: a review. *Smart Mater Struct* 2016; 25(5): 053001.
2. SAE International. Guidelines for implementation of structural health monitoring on fixed wing aircraft. SAE paper ARP6461, 2013.
3. Aldrin J, Medina E, Lindgren E, et al. Protocol for reliability assessment of structural health monitoring systems incorporating model-assisted probability of detection (MAPOD) approach. In: *Proceedings of the 8th international workshop on structural health monitoring*, Stanford, 13–15 September 2011, pp. 1–8. Lancaster, PA: DEStech Publications.
4. US Department of Defense. *Military handbook 1823: nondestructive evaluation of system reliability assessment*. Washington, DC: US Department of Defense, 2009.
5. Berens AP. NDE reliability data analysis. *ASM Handbook* 1989; 17: 689–701.
6. Buethe I, Dominguez N, Jung H, et al. Path-based MAPOD using numerical simulations. In: Wölcken PC and Papadopoulos M (eds) *Smart intelligent aircraft structures (SARISTU)*. New York: Springer, 2016, pp. 631–642.
7. Eckstein B, Fritzen CP and Bach M. Considerations on the reliability of guided ultrasonic wave-based SHM systems for CFRP aerospace structures. In: *Proceedings of the 6th European workshop on structural health monitoring*, Dresden, 3–6 July 2012, pp. 957–964.
8. Moix-Bonet M, Eckstein B, Bach M, et al. Damage classification in aeronautic structures using guided waves. In: *Proceedings of the 11th international workshop on structural health monitoring*, Stanford, CA, 12–14 September 2017.
9. Shen Y and Cesnik CES. Modeling guided wave propagation in composite structures using local interaction simulation approach. In: Liu WK, Hutchings I and Huiskes R. (eds) *Computational and experimental methods in structures*, vol. 8. London: World Scientific Publishing, 2018, pp. 47–91.
10. Leckey CA, Wheeler KR, Hafiychuk VN, et al. Simulation of guided-wave ultrasound propagation in composite laminates: benchmark comparisons of numerical codes and experiment. *Ultrasonics* 2018; 84: 187–200.
11. Bulling J, Prager J and Korme F. Application of the Scaled Boundary Finite Element Method (SBFEM) for a numerical simulation of ultrasonic guided waves, 2017, https://www.ama-science.org/proceedings/details/2603
12. Glushkov EV, Glushkova NV, Eremin AA, et al. Ultrasonic guided wave characterization and inspection of laminate fiber-reinforced composite plates. In: Parinov IA, Chang SH and Topolov VY (eds) *Advanced materials*. Cham: Springer, 2016, pp. 449–457.
13. Samaratunga D, Jha R and Gopalakrishnan S. Wavelet spectral finite element for modeling guided wave propagation and damage detection in stiffened composite panels. *Struct Health Monit* 2016; 15(3): 317–334.
14. Ostachowicz WM, Kudela P, Krawczuk M, et al. *Guided waves in structures for SHM: the time-domain spectral element method*. Hoboken, NJ: John Wiley & Sons, 2012.
15. Schulte R, Fritzen CP and Moll J. Spectral element modelling of wave propagation in isotropic and anisotropic shell-structures including different types of damage. *IOP Conf Ser: Mater Sci Eng* 2010; 10(1): 012065.
16. Moser F, Jacobs LJ and Qu J. Modeling elastic wave propagation in waveguides with the finite element method. *NDT&E Int* 1999; 32(4): 225–234.
17. Michaels JE. Ultrasonic wavefield imaging. In: Ida N and Meyendorf N (eds) *Handbook of advanced non-destructive evaluation*. Cham: Springer, 2018, pp. 1–32.
18. Yu L, Tian Z, Li X, et al. Core–skin debonding detection in honeycomb sandwich structures through guided wave wavefield analysis. *J Intel Mater Syst Struct*. Epub ahead of print 27 February 2018. DOI: 10.1177/1045389X1875 8180.
19. Harley JB and Chia CC. Statistical partial wavefield imaging using Lamb wave signals. *Struct Health Monit* 2018; 17(4): 919–935.
20. Keshmiri Esfandabadi Y, De Marchi L, Testoni N, et al. Full wavefield analysis and damage imaging through compressive sensing in lamb wave inspections. *IEEE T Ultrason Ferr* 2018; 65(2): 269–280.

21. De Marchi L, Marzani A, Moll J, et al. A pulse coding and decoding strategy to perform Lamb wave inspections using simultaneously multiple actuators. *Mech Syst Signal Pr* 2017; 91: 111–121.

22. Flynn EB, Chong SY, Jarmer GJ, et al. Structural imaging through local wavenumber estimation of guided waves. *NDT&E Int* 2013; 59: 1–10.

23. Kudela P, Radzienski M, Ostachowicz W, et al. Structural health monitoring system based on a concept of Lamb wave focusing by the piezoelectric array. *Mech Syst Signal Pr* 2018; 108: 21–32.

24. Alguri KS, Melville J and Harley JB. Baseline-free guided wave damage detection with surrogate data and dictionary learning. *J Acoust Soc Am* 2018; 143(6): 3807–3818.

25. Memmolo V, Maio L, Boffa ND, et al. Damage detection tomography based on guided waves in composite structures using a distributed sensor network. *Optical Eng* 2015; 55(1): 011007.

26. Lee SJ, Gandhi N, Hall JS, et al. Baseline-free guided wave imaging via adaptive source removal. *Struct Health Monit* 2012; 11(4): 472–481.

27. Moll J, Schulte R, Hartmann B, et al. Multi-site damage localization in anisotropic plate-like structures using an active guided wave structural health monitoring system. *Smart Mater Struct* 2010; 19(4): 045022.

28. Wierach P, Monner HP, Schoenecker A, et al. *Application-specific design of adaptive structures with piezoceramic patch actuators.* San Diego, CA: SPIE, 2002, pp. 333–341.

29. Schnars U and Henrich R. Applications of NDT methods on composite structures in aerospace industry. In: *Proceedings of the conference on damage in composite materials*, Stuttgart, 2006, pp. 1–8.

30. Brandt C and Maaß P. A state space approach for the non-destructive evaluation of CFRP with ultrasonic testing. In: *Proceedings of the 7th international symposium on NDT in aerospace*, 2016, pp. 1–8.

31. Singhal A, Grande JC and Zhou Y. Micro/nano-CT for visualization of internal structures. *Microscop Today* 2013; 21(2): 16–22.

32. Petersen E, Cuntze R and Hühne C. Experimental determination of material parameters in Cuntze's failure-mode-concept-based UD strength failure conditions. *Compos Sci Technol* 2016; 134: 12–25.

33. Sause MGR. Digital image correlation. In: Sause MGR (ed.) *In situ monitoring of fiber-reinforced composites*, vol. 242. Cham: Springer, 2016, pp. 57–129.

34. Schürmann H. *Konstruieren mit Faser-Kunststoff-Verbunden.* 2nd ed. Berlin: Springer, 2007.

35. Sause MGR. Acoustic emission. In: Sause MGR (ed.) *In situ monitoring of fiber-reinforced composites*, vol. 242. Cham: Springer, 2016, pp. 131–359.

36. Torres Arredondo M, Ramirez Lozano M and Fritzen CP. *DispWare toolbox—a scientific computer program for the calculation of dispersion relations for modal-based acoustic emission and ultrasonic testing* (technical report). Siegen: University of Siegen, 2011.

37. Torres Arredondo M. *Acoustic emission testing and acousto-ultrasonics for structural health monitoring.* PhD Thesis, University of Siegen, Siegen, 2013.

38. Rose JL. A baseline and vision of ultrasonic guided wave inspection potential. *J Press Vess T ASME* 2002; 124(3): 273.

39. Su Z, Ye L and Lu Y. Guided Lamb waves for identification of damage in composite structures: a review. *J Sound Vib* 2006; 295(3–5): 753–780.

40. Wang L and Yuan F. Group velocity and characteristic wave curves of Lamb waves in composites: modeling and experiments. *Compos Sci Technol* 2007; 67(7–8): 1370–1384.

41. Ramadas C, Balasubramaniam K, Joshi M, et al. Interaction of the primary anti-symmetric Lamb mode (A0) with symmetric delaminations: numerical and experimental studies. *Smart Mater Struct* 2009; 18(8): 085011.

42. Abrate S. Impact on laminated composite materials. *Appl Mech Rev* 1991; 44(4): 155.

43. Sedov A, Schmerr LW and Song SJ. Ultrasonic scattering by a flat-bottom hole in immersion testing: an analytical model. *J Acoust Soc Am* 1992; 92(1): 478–486.

44. Beard SJ, Kumar A, Qing X, et al. *Practical issues in real-world implementation of structural health monitoring systems.* San Diego, CA: SPIE, 2005, p. 196.

45. Bach M, Pouilly A, Eckstein B, et al. Reference damages for verification of probability of detection with guided waves. In: Chang FK and Kopsaftopoulos F (eds) *Structural health monitoring*. Lancaster, PA: DEStech Publications, 2017.

46. Giurgiutiu V. Tuned lamb wave excitation and detection with piezoelectric wafer active sensors for structural health monitoring. *J Intell Mater Syst Struct* 2005; 16(4): 291–305.

47. Neuschwander K, Moll J, Memmolo V, et al. Simultaneous load and structural monitoring of a carbon fiber rudder stock: results from a quasi-static tensile test. *J Intell Mater Syst Struct.* Epub ahead of print 26 March 2018. DOI: 10.1177/0954406218764226.

48. Neuschwander K, Shrestha A, Moll J, et al. Multichannel device for integrated pitch catch and EMI measurements in guided wave structural health monitoring applications. In: *Proceedings of the 11th international workshop on structural health monitoring*, Stanford, CA, 12–14 September 2017, pp. 1723–1730. DEStech Publications, Inc.

49. Attarian VA, Cegla FB and Cawley P. Long-term stability of guided wave structural health monitoring using distributed adhesively bonded piezoelectric transducers. *Struct Health Monit* 2014; 13(3): 265–280.

50. Croxford A, Moll J, Wilcox P, et al. Efficient temperature compensation strategies for guided wave structural health monitoring. *Ultrasonics* 2010; 50(4–5): 517–528.

51. Douglass ACS and Harley JB. Dynamic time warping temperature compensation for guided wave structural health Monitoring. *IEEE T Ultrason Ferr* 2018; 65(5): 851–861.

52. Hay TR, Royer RL, Gao H, et al. A comparison of embedded sensor Lamb wave ultrasonic tomography approaches for material loss detection. *Smart Mater Struct* 2006; 15(4): 946–951.